Available online at www.sciencedirect.com
ScienceDirect
Journal of Sound and Vibration 320 (2009) 1004–1022
JOURNAL OF SOUND AND VIBRATION
www.elsevier.com/locate/jsvi

A novel scheme for the discrete prediction of high-frequency vibration response: Discrete singular convolution–mode superposition approach

Abdullah Seçgin*, A. Saide Sarıgül

Department of Mechanical Engineering, Dokuz Eylül University, 35100 Bornova, İzmir, Turkey

Received 26 February 2008; received in revised form 4 June 2008; accepted 13 August 2008
Handling Editor: C.L. Morfey
Available online 7 October 2008

Abstract

This study introduces a novel scheme for the discrete high-frequency forced vibration analysis based on discrete singular convolution (DSC) and mode superposition (MS) approaches. The accuracy of the DSC–MS is validated for thin beams and plates by comparing with available analytical solutions. The performance of the DSC–MS is evaluated by predicting spatial distribution and discrete frequency spectra of the vibration response of thin plates with two different boundary conditions. The frequency spectra of the time-harmonic excitation forces are in the form of ideal and band-limited white noise so that the natural modes in the frequency band are provoked. The solution exposes high-frequency response behaviour definitely. Therefore, it is hoped with this paper to contribute the studies on the treatment of uncertainties in the high-frequency design applications.

1. Introduction

In the science of vibro-acoustics, vibration and acoustic problems are classified according to their frequency range as, low-, medium- and high-frequency problems. Since dynamic behaviour of systems changes with regard to the excitation frequency, adaptive approaches are required for reliable solutions. In practice, it is not mentioned about definite boundaries separating frequency ranges from each other due to the fact that they may change from system to system. However, Rabbiolo et al. [1] have put forward an indicator for approximately defining high-frequency thresholds based on "modal overlap count (modal overlap factor)" of simple structures such as beams, plates and acoustical spaces. It is known that modelling high-frequency dynamic systems using deterministic techniques such as finite element method (FEM) and boundary element method (BEM) is numerically expensive. Besides, since the vibro-acoustic response is very sensitive to the changes in system parameters at higher frequencies, some uncertainties are encountered. Therefore, deterministic techniques are feasible only for low-frequency analysis. Albeit hierarchical FEM (p-FEM) has

*Corresponding author. Tel.: +90 232 3887868; fax: +90 232 3887864.
E-mail addresses: abdullah.secgin@deu.edu.tr (A. Seçgin), saide.sarigul@deu.edu.tr (A. Saide Sarıgül).

0022-460X/$ - see front matter © 2008 Elsevier Ltd. All rights reserved.
doi:10.1016/j.jsv.2008.08.031

extended the frequency limit of classical FEM and this approach is generally regarded as mid-frequency technique.

The statistical energy analysis (SEA) developed by Lyon and Maidanik in 1962 has proved its validity for high-frequency analysis [2]. However, SEA is based on some pre-assumptions restricting its efficiency and capacity. Therefore, several alternative energy-based techniques have been developed [3–11]. Among them, energy flow analysis (EFA) and its finite element application, energy finite element method (EFEM) are common approaches in service [3–6]. However, since all these methods consider average prediction of energy as system variable to describe the response level, they disregard modal information and thus, loose discrete frequency response behaviour of the structure. Specifically, as far as the present authors are aware, any high-frequency method is not present in order to predict frequency response discretely without missing modal information and so being a key for high-frequency uncertainties. Furthermore, there is not any unique method valid for all frequency ranges to perform response analysis.

In the last decade, a novel approach called discrete singular convolution (DSC) has been introduced by Wei [12–15]. This is a powerful method for the numerical solution of differential equations. The solution technique of the DSC is based on the theory of distribution and wavelets. This approach has been successfully used in various free vibration analyses of isotropic thin simple structures with several boundary conditions [16–24]. Hou et al. [25] have used DSC–Ritz method for the free vibration analysis of thick plates. Civalek [26–28] has applied the DSC to the free vibration and buckling analyses of different laminated shells and plates. Seçgin et al. [29] have used the DSC for the free vibration of fiber–metal laminated composite plates. Seçgin and Sarıgül [30] have presented open algorithm of the DSC and have shown the superiority of the DSC over several numerical techniques for the free vibration analysis of symmetrically laminated composite plates. Moreover, for high-frequency free vibration analysis, Wei et al. [31] and Zhao et al. [32] have obtained ten thousands of vibration modes for thin beams and plates. Lim et al. [33] have used DSC–Ritz approach for high-frequency modal analysis of thick shells. Ng et al. [34] have pointed out that the DSC yields more accurate prediction compared to differential quadrature method for the plates vibrating at high frequencies. These successes of the DSC promise that this method would be reliably used for discrete high-frequency response analysis without handling averaged energetic parameters unlike the available high-frequency approaches.

In this regard, the present paper introduces a novel scheme for the discrete high-frequency forced vibration analysis by employing discrete singular convolution (DSC) and mode superposition (MS) approaches. Although at high frequencies thin-structure theories may be hardly satisfied, in order to avoid the additional complexity caused by thick-structure theories, simple physical models were used for the introduction of the present scheme as done in Refs. [31,32]. The validation of the scheme is realized by the comparisons with the analytical solutions of spatially distributed response of beams and frequency response of infinite plates. Besides, performance and restrictions of DSC–MS approach are discussed by the demonstrations of spatial distribution and frequency spectra of the vibration response for a wide frequency range. The frequency spectra of the time-harmonic point-excitation forces are in the form of ideal and band-limited white noise, so that the natural modes in the considered frequency region are excited. These discrete modes appearing in the response spectra are pleasant signals of recovering the uncertainties of high-frequency applications.

2. Discrete singular convolution (DSC)

Singular convolution is defined by the theory of distributions. Let T be a distribution and $\eta(t)$ be an element of the space of test functions. Then, a singular convolution can be given by [12]

$$F(t) = (T * \eta)(t) = \int_{-\infty}^{\infty} T(t-x)\eta(x)\,\mathrm{d}x \tag{1}$$

Here, the sign $*$ is the convolution operator, $F(t)$ is the convolution of η and T, $T(t-x)$ is the singular kernel of the convolution integral. Depending on the form of the kernel T, singular convolution can be applied to different science and engineering problems. Delta kernel is an interpolation function essential for the numerical solution of partial differential equations:

$$T(x) = \delta^n(x) \quad n = 0, 1, 2, \ldots \tag{2}$$

Delta kernels given in Eq. (2) are proper for use in vibration analysis. However, these kernels are singular; thus, they can not be digitized directly in computer. In order to avoid this problem, sequences of approximations T_α of the distributions T can be constructed such that T_α converge to T:

$$\lim_{\alpha\to\alpha_0} T_\alpha(x) \to T(x) \tag{3}$$

where α_0 is a generalized limit. With a good approximation, a DSC can be determined as

$$F_\alpha(x) = \sum_k T_\alpha(x - x_k) f(x_k) \tag{4}$$

Here, $F_\alpha(x)$ is an approximation to $F(x)$ and $\{x_k\}$ is an approximate set of discrete points on which the DSC in Eq. (4) is well defined. $f(x)$ is used here as the test function replacing the original test function $\eta(x)$. A sequence of approximation can be improved by a regularizer in order to increase the regularity of convolution kernels. Gaussian regularizer is a typical delta regularizer and it is in the form of

$$R_\sigma(x) = \mathrm{e}^{-x^2/2\sigma^2} \tag{5}$$

where σ is the standard deviation. Delta kernel with sampling parameter α approximately in the form

$$T_\alpha = \frac{\sin\ \alpha x}{\pi x} \tag{6}$$

is known as Shannon father wavelet (scaling function). In vibration analysis, a discretized form of Eq. (6), which is sampled by Nyquist frequency ($\alpha = \pi/\Delta$, Δ is the grid spacing) and improved by Gaussian regularizer, can be chosen as the kernel function of the DSC [12]

$$\delta_{\pi/\Delta,\sigma}(x - x_k) = \frac{\sin[\pi/\Delta(x - x_k)]}{\pi/\Delta(x - x_k)} \exp(-(x - x_k)^2/2\sigma^2) \tag{7}$$

Here, Δ is determined by considering required precision of the analysis. The DSC expression in Eq. (4) can be rewritten by using regularized Shannon delta kernel (RSDK) given in Eq. (7):

$$f(x) \approx \sum_{k=-\infty}^{\infty} \frac{\sin[\pi/\Delta(x - x_k)]}{\pi/\Delta(x - x_k)} \exp(-(x - x_k)^2/2\sigma^2) f(x_k) \tag{8}$$

As seen in Eq. (8), since DSC approach is defined in an infinite region, the kernels must be bounded in a sufficient computational domain for numerical determination. This can be practically achieved by a spatial truncation of the convolution kernel. A translationally invariant symmetric truncation algorithm can be used in an efficient bandwidth $(2M+1)$ as follows:

$$f^{(n)}(x_m) \approx \sum_{k=-M}^{M} \delta^{(n)}_{\pi/\Delta,\sigma}(x_m - x_k) f(x_k) \tag{9}$$

Here, x_m is the specific central point considered and $\delta^{(n)}_{\pi/\Delta,\sigma}(x)$ is the nth derivative of $\delta(x)$ given in Eq. (7) with respect to x.

3. DSC–MS scheme

3.1. MS technique for plates

MS technique assumes a solution that all system modes discretely contribute to local displacement response. The mathematical foundation of the MS is based on the separation of variables. Bending displacement response of a plate $w(x,y,t)$ can be expressed by the infinite summation of the product of two variables; $\phi_p(x,y)$, the pth natural mode shape of the plate and $w_p(t)$, the magnitude of the pth mode [35]:

$$w(x, y, t) = \sum_{p=1}^{\infty} w_p(t)\phi_p(x, y) \tag{10}$$

Eq. (10) can be approximately written in terms of sufficient number of modes P contributing the response:

$$w(x,y,t) \approx \sum_{p=1}^{P} w_p(t)\phi_p(x,y) \tag{11}$$

The equation of bending motion of a thin plate with internal loss factor $\zeta<1$ is given in terms of the displacement w:

$$D^2(1+\mathrm{j}\zeta)\nabla^4 w(x,y,t) + \ddot{w}(x,y,t) = \frac{1}{\rho h} f(x,y,t) \tag{12}$$

where $D^2 = D_0/\rho h$ ($D_0 = Eh^3/12(1-\upsilon^2)$is the plate rigidity, E: modulus of elasticity, h: plate thickness, υ: Poisson's ratio), ρ is mass density, $\mathrm{j} = \sqrt{-1}$ and $\nabla^4 = (\partial^4/\partial x^4 + 2\partial^4/\partial x^2\partial y^2 + \partial^4/\partial y^4)$. By applying Eq. (11) to the homogenous part of Eq. (12) yields

$$D^2(1+\zeta^2)\sum_{p=1}^{P} \nabla^4\phi_p(x,y)w_p(t) + (1-\mathrm{j}\zeta)\sum_{p=1}^{P} \phi_p(x,y)\ddot{w}_p(t) = 0 \tag{13}$$

Eq. (13) leads to the following equations:

$$D^2(1+\zeta^2)\sum_{p=1}^{P} \nabla^4\phi_p(x,y)\frac{1}{\phi_p(x,y)} = -(1-\mathrm{j}\zeta)\sum_{p=1}^{P} \ddot{w}_p(t)\frac{1}{w_p(t)} = \sum_{p=1}^{P} k_p \tag{14}$$

$$D^2(1+\zeta^2)\sum_{p=1}^{P} \nabla^4\phi_p(x,y) - \sum_{p=1}^{P} k_p\phi_p(x,y) = 0 \tag{15}$$

$$(1-\mathrm{j}\zeta)\sum_{p=1}^{P} \ddot{w}_p(t) + \sum_{p=1}^{P} k_p w_p(t) = 0 \tag{16}$$

Here k_p is always a positive number which represents the square of the natural frequency of the pth mode, ω_p.

For multi-excitations, point force $f(x,y,t) = \sum_{i=1}^{N}\sum_{j=1}^{N} f_{i,j}(t)\delta(x-x_i)\delta(y-y_j)$ (δ is the Dirac-delta function) can be identified as

$$f(x,y,t) = \sum_{p=1}^{P}\left(\sum_{i=1}^{N}\sum_{j=1}^{N} f_{i,j}(t)\phi_p(x_i,y_j)\right) \tag{17}$$

3.2. DSC discretization

It is useful to define the following indices in the determination of the entire DSC domain for r direction of differentiation ($r = x$ or y for plates):

$$k = -M,\ldots,0,\ldots,M; \quad i_r = 0,1,2,\ldots,N_r-1; \quad j_r = -M,\ldots,0,\ldots,N_r-1+M \tag{18}$$

where N_r represents the number of structure points whereas M denotes the number of auxiliary points with the condition that $N_r \geqslant M+1$. Structure and auxiliary points are positioned by the same uniform interval Δ_r. Consequently, DSC expression given in Eq. (9) is rewritten in the discretized domain as

$$F^{(n)}(r_{i_r}) \approx \sum_{k=-M}^{M} \delta^{(n)}_{\pi/\Delta,\sigma}(k\Delta_r)F(r_{i_r+k}) \tag{19}$$

where $k\Delta_r = (r_0 - r_k) = (r_1 - r_k) = \cdots = (r_{N_r-1} - r_k)$.

3.3. DSC–MS implementation

Defining a full mode shape function $\Phi_f = \sum_{p=1}^{P} \phi_p$ and applying DSC expression in Eqs. (19)–(15) by introducing the non-dimensional parameters; $X = x/a$, $Y = y/b$, $\Phi = \Phi_f a$, $\lambda = a/b$, $\Omega = \omega a^2/D\sqrt{1+\zeta^2}$ yields:

$$\sum_{k=-M}^{M} \delta^{(4)}_{\pi/\Delta_x,\sigma}(k\Delta_x)\Phi(X_{i_x+k}, Y) + 2\lambda^2 \sum_{k=-M}^{M} \delta^{(2)}_{\pi/\Delta_x,\sigma}(k\Delta_x)\Phi(X_{i_x+k}, Y) \sum_{k=-M}^{M} \delta^{(2)}_{\pi/\Delta_y,\sigma}(k\Delta_y)\Phi(X, Y_{i_y+k}) + \lambda^4 \sum_{k=-M}^{M} \delta^{(4)}_{\pi/\Delta_y,\sigma}(k\Delta_y)\Phi(X, Y_{i_y+k}) = \mathbf{\Omega}^2\Phi(X, Y) \tag{20}$$

Here, $\mathbf{\Omega}$ is the diagonal natural frequency parameter matrix. The mode shape vector of the plate is formed as

$$\mathbf{\Phi} = \{\Phi_{0,0}, \ldots, \Phi_{0,N_y-1}, \Phi_{1,0}, \ldots, \Phi_{1,N_y-1}, \ldots, \ldots, \Phi_{N_x-1,0}, \ldots, \Phi_{N_x-1,N_y-1}\}^{\mathrm{T}} \tag{21}$$

This discretization is illustrated in Fig. 1. DSC kernels in Eq. (20) can be written in a DSC matrix form as

$$\Psi^{(n)}_{r\,i_r,j_r} = \begin{cases} \delta^{(n)}_{\pi/\Delta_r,\sigma}((j_r - i_r)\Delta_r), & \text{if } -M \leqslant j_r - i_r \leqslant M \\ 0, & \text{otherwise} \end{cases} \tag{22}$$

The numerical scheme of the DSC–MS is completed by implementing the boundary conditions to Eq. (20). For simply supported and clamped boundary conditions, an assumption on the relation between auxiliary points and structure points can be made by determining an arbitrary index $S = 1, \ldots, M$ and the coefficients $A_{r,s}$ and $B_{r,s}$:

For left ($r = X$) and top ($r = Y$) boundaries

$$\Phi(r_{-s}) - \Phi(r_0) = A_{r,s}[\Phi(r_s) - \Phi(r_0)] \tag{23}$$

In a similar way, for right ($r = X$) and bottom ($r = Y$) boundaries

$$\Phi(r_{N_r-1+s}) - \Phi(r_{N_r-1}) = B_{r,s}[\Phi(r_{N_r-1-s}) - \Phi(r_{N_r-1})] \tag{24}$$

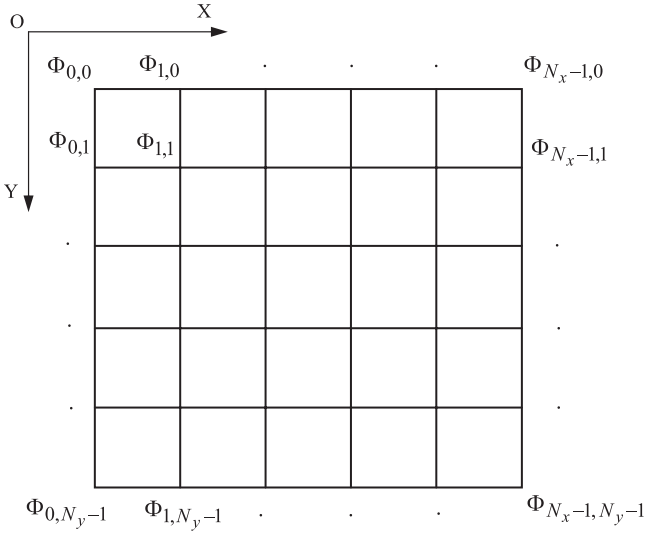

Fig. 1. DSC grid representation for plates.

Any auxiliary point can be written in terms of structure points by using one of the relations in Eqs. (23) and (24). Then by using the DSC expression in Eq. (19), one can obtain the coefficients as $A_{r,s} = B_{r,s} = -1$ for SSSS and $A_{r,s} = B_{r,s} = 1$ for CCCC plates, for each s value. For these plates, after implementation of the displacement boundary condition $\Phi(r_0) = \Phi(r_{N-1}) = 0$, Eq. (20) can be reconstructed by DSC matrices as an eigenvalue equation:

$$(\mathbf{T} - \boldsymbol{\Omega}^2)\Phi = 0 \tag{25}$$

Here $\mathbf{T}$ matrix can be expressed as

$$\mathbf{T} = \left\{(\boldsymbol{\Gamma}_x^{(4)} \otimes \mathbf{I}_y) + 2\lambda^2(\boldsymbol{\Gamma}_x^{(2)} \otimes \boldsymbol{\Gamma}_y^{(2)}) + \lambda^4(\mathbf{I}_x \otimes \boldsymbol{\Gamma}_y^{(4)})\right\} \tag{26}$$

where $\boldsymbol{\Gamma}_r^{(n)}$ is the DSC characteristic matrix, $\mathbf{I}_r$ is the identity matrix, and the symbol $\otimes$ denotes tensorial product. For square plates $\lambda = 1$; $\mathbf{I}_x = \mathbf{I}_y$. A characteristic matrix is obtained by applying specific boundary conditions to the DSC matrix $\boldsymbol{\Psi}_r^{(n)}{}_{N\times(2M+N)}$ defined in Eq. (22). From Eq. (25), one can obtain natural frequencies ($\omega_1, \omega_2, \ldots, \omega_P$) and the corresponding mode shapes ($\phi_1, \phi_2, \ldots, \phi_P$).

Eq. (16) can be reconstructed by the force term:

$$(1 - \mathrm{j}\zeta)\sum_{p=1}^{P}(\ddot{w}_p(t) + \omega_p^2 w_p(t)) = \frac{1}{\rho h}\sum_{p=1}^{P}\left(\sum_{i=1}^{N}\sum_{j=1}^{N} f_{i,j}(t)\phi_p(x_i, y_j)\right) \tag{27}$$

Assuming a harmonic response in the form of $w_p(t) = W_p \mathrm{e}^{\mathrm{i}\omega t}$, the steady-state frequency response can be obtained as follows:

$$W_p(\omega) = \frac{1}{\rho h}\sum_{p=1}^{P}\left(\frac{1}{\omega_p^2 - (1 - \mathrm{j}\zeta)\omega^2}\sum_{i=1}^{N}\sum_{j=1}^{N} F_{i,j}(\omega)\phi_p(x_i, y_j)\right) \tag{28}$$

where $F_{i,j}(\omega)$ is the Fourier transform of $f_{i,j}(t)$. Substituting Eq. (28) into Fourier transform of Eq. (11), one can obtain a space-frequency dependent response equation for thin plates as follows:

$$W(x, y, \omega) = \frac{1}{\rho h}\sum_{p=1}^{P}\left(\frac{\phi_p(x, y)}{\omega_p^2 - (1 - \mathrm{j}\zeta)\omega^2}\sum_{i=1}^{N}\sum_{j=1}^{N} F_{i,j}(\omega)\phi_p(x_i, y_j)\right) \tag{29}$$

4. Numerical study

This section has been organized as four main parts. The first part is concerned with the high-frequency concept. The second part includes a convergence study for the DSC predictions of thin beams and plates. The third part presents verification study of DSC–MS approach by comparisons of vibration response predictions of thin beams and plates with analytical solutions. The last part concentrates on the performance of the DSC–MS for discrete response analysis of thin plates by presentations of several numerical applications.

4.1. High-frequency concept

In vibro-acoustics, modal overlap count is an indicator of the threshold of high-frequency region. This count is defined as [1]

$$\mathrm{MO} = \frac{\Delta f_n}{\delta f} = \frac{\zeta f_n}{\delta f} \tag{30}$$

Here, f_n is the natural frequency, Δf_n is the modal bandwidth and δf is the average modal spacing between two adjacent modes in the frequency bandwidth. A schematic representation of these parameters is given in Fig. 2. Rabbiolo et al. [1] have defined three different high-frequency thresholds based upon the approximate modal overlap counts; $\overline{\mathrm{MO}} = 1$ for beams, $\overline{\mathrm{MO}} = 2.5$ for plates and $\overline{\mathrm{MO}} = 3$ for acoustic enclosures.

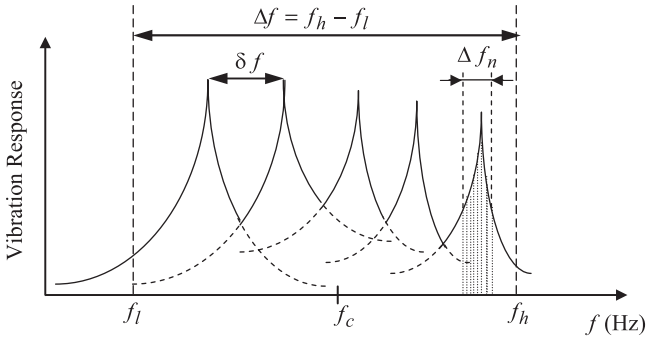

Fig. 2. Representation of modal parameters in a bandwidth.

Modal overlap count is also defined by the centre frequency, f_c and the modal density, $n(f)$ of a considered bandwidth as follows [36]:

$$\mathrm{MO} = \zeta f_c n(f) \tag{31}$$

Modal density is the number of modes in a considered frequency bandwidth i.e., $n(f) = P/\Delta f$. For simple structures, modal density can be analytically determined. For instance, modal density for plates is given as [37]

$$n(\omega) = \frac{A_s}{4\pi\sqrt{D_0/\rho h}} \tag{32}$$

where A_s is the surface area of the plate and it is noted that $n(f) = 2\pi n(\omega)$. Generally, if MO given in Eq. (31) is higher than unity, the energy-based approaches such as SEA and EFEM can be reliably used in this region [38]. Eqs. (30) and (31) indicate that the modal overlap count is determined only for damped systems with a sufficiently wide frequency band. Therefore, for an undamped system solution the modal overlap count cannot be used as an indicator of high-frequency range.

4.2. Convergence study of DSC approach

Although, a comprehensive convergence study for very higher modes was given by Wei et al. [31], a brief demonstration for the accuracy of the DSC is also presented in this study by using three different number of discretization point N associated with three different discretization parameter r. Here, the relative error is defined as % error $= 100 \times (\Omega_A - \Omega_D)/\Omega_A$, where Ω_A and Ω_D are non-dimensional frequency parameters obtained by analytical and DSC solutions, respectively.

The discretization parameter r is defined as a ratio that depends on the regularization parameter σ and the discretization interval Δ, i.e., $r = \sigma/\Delta$. In addition to the selection of high number of discretization points, a reliable modal prediction also directly depends on the appropriate selection of discretization parameter. However, adapting very low and very high r values may cause some numerical instability. A proper selection can be made by trial and error method. Actually, Qian and Wei [39] have presented a mathematical estimation for the relative selection of r, σ and M in a reliable wide range. Brief statements for this estimation can also be found in Refs. [18,20,22].

Figs. 3(a–c) show relative error for frequency parameters of simply supported beams whereas Figs. 4(a–i) present errors for simply supported plates. In the given convergence tests, r values were selected as 4.1–8.1, 6.1–10.1 and 8.1–12.1 corresponding to $N = 1001$, 2001 and 3001 respectively, for beams; and corresponding to $N = 51 \times 51$, $N = 61 \times 61$ and $N = 71 \times 71$ respectively, for plates.

As Figs. 3(a–c) are examined, it is clearly seen that increasing r decreases the relative errors for each of N values and also increasing N decreases the error values of the considered modes. For $N = 3001$ with $r = 12.1$, the first 2999 natural modes of beams can be obtained by maximum error of 0.018%. However, $N = 1001$ grid points corresponding the first 999 natural modes state the error under 0.07%, independent of r value. Actually, this score is also reliable for high-frequency analysis. The same effect of r is also realized for plates as Figs. 4(a–i) are examined. The first 4761 modes are accurately obtained for $N = 71 \times 71$ with $r = 12.1$; and

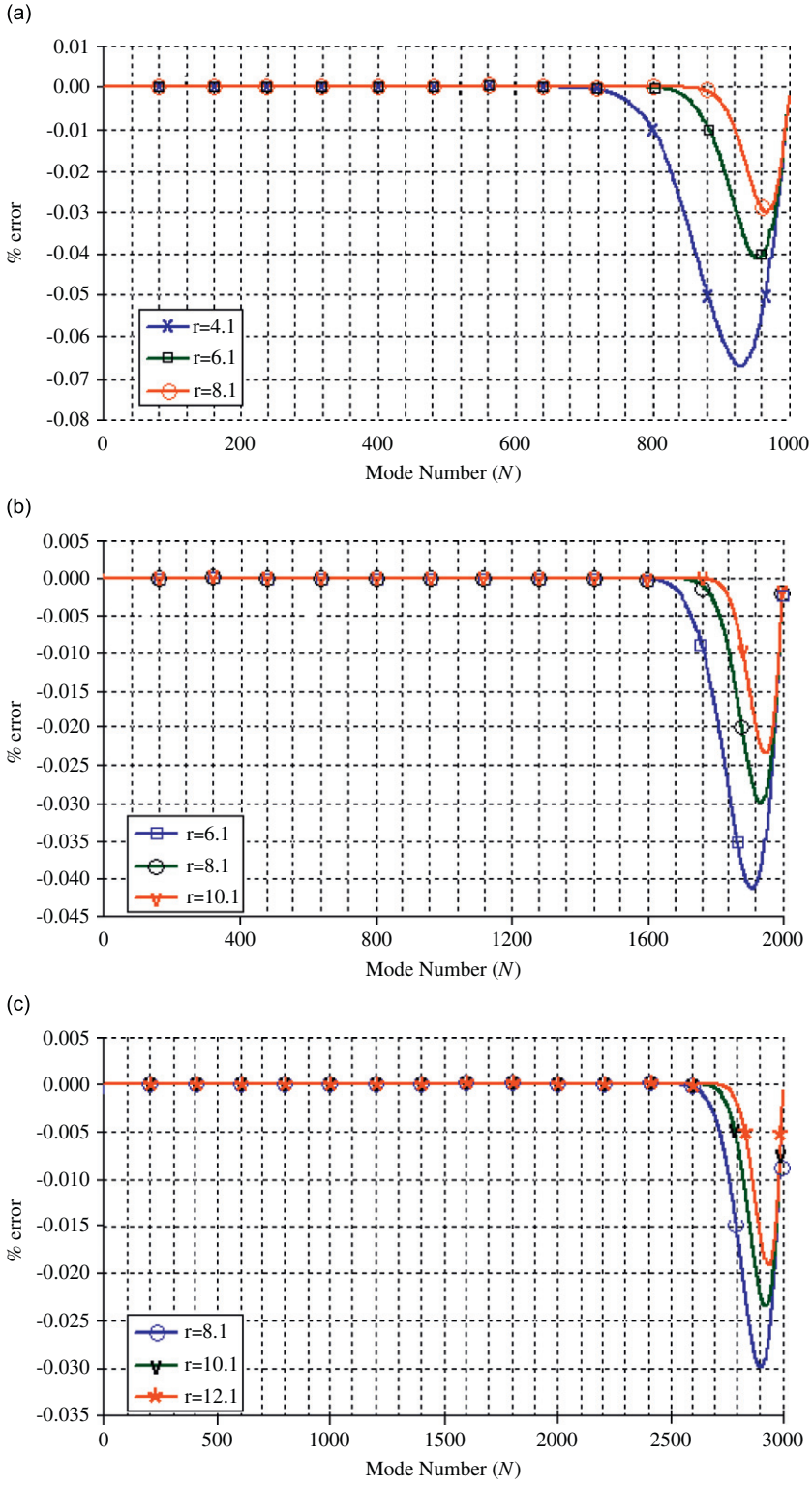

Fig. 3. Convergence test for DSC modal predictions of beams.

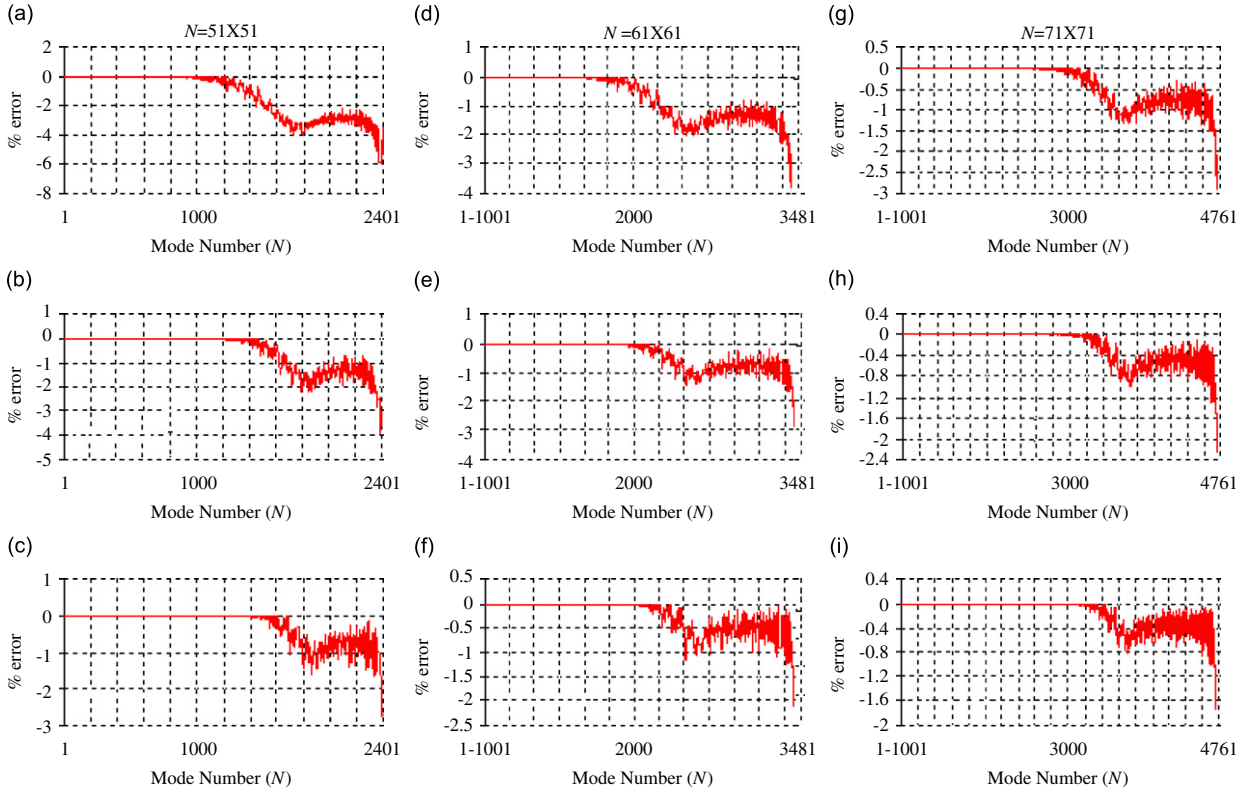

Fig. 4. Convergence test for DSC modal predictions of plates. (a) $r = 4.1$, (b) $r = 6.1$, (c) $r = 8.1$, (d) $r = 6.1$, (e) $r = 8.1$, (f) $r = 10.1$, (g) $r = 8.1$, (h) $r = 10.1$ and (i) $r = 12.1$.

approximately 1% error is observed for the first 4750. Selecting $N = 51 \times 51$ for each r, predicts at least the first 1000 modes with zero error. This amount of modes also indicates high-frequency region.

4.3. Verification of DSC–MS approach

4.3.1. Vibration displacement response of a thin beam

Analytical solution for the displacement response of a simply supported undamped beam subjected to a point force F applied at the centre is [40]

$$w(x,t) = \frac{2F}{\rho A a} \sum_{n=1}^{\infty} \frac{\sin(n\pi/2)}{\omega_n^2(1-(\omega/\omega_n)^2)} \frac{\sin(n\pi x)}{a} \sin(\omega t) \tag{33}$$

where

$$\omega_n^2 = \frac{n^4\pi^4 EI}{\rho A a^4}, \quad n = 1,2,3,\ldots. \tag{34}$$

Here a is the beam length, I is the moment of inertia and A is the area of the beam cross-section. In the analysis, the beam was discretized by $N = 3001$ grid points with $r = 12.1$ providing $P = 2999$ natural modes. A harmonic point force in the form of $F = 100\sin(200\,\pi t)$ N was applied. The physical properties of the beam are: $a = 1\,\text{m}$, $\rho = 2700\,\text{kg/m}^3$, $A = 1 \times 10^{-4}\,\text{m}^2$, $E = 7.1 \times 10^{10}\,\text{N/m}^2$, $I = 8.33 \times 10^{-10}\,\text{m}^4$ and the natural frequency parameters are given as

$$\Omega_n = \omega_n \sqrt{\frac{\rho A}{EI}} = \left(\frac{n\pi}{a}\right)^2, \quad n = 1,2,3,\ldots. \tag{35}$$

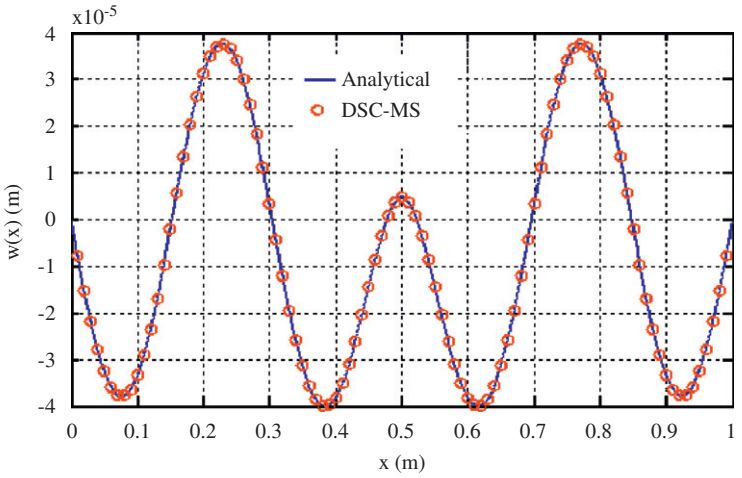

Fig. 5. Comparison of the spatially distributed displacement response predicted by the DSC–MS with analytical results for simply supported beam with $\zeta = 0$.

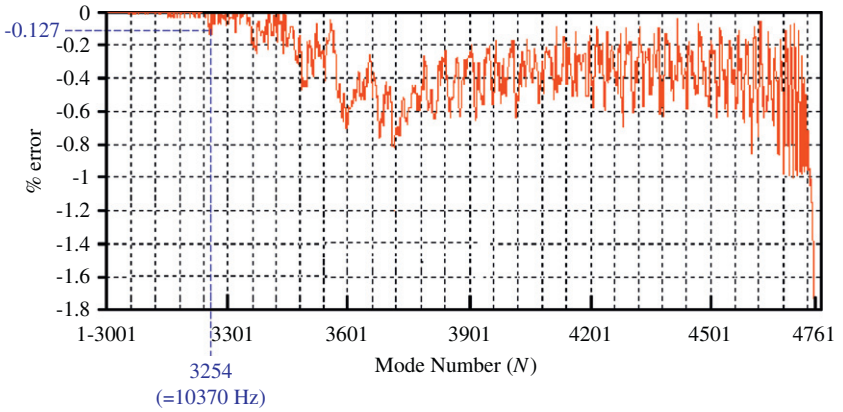

Fig. 6. Relative error of DSC solutions compared to the analytical results for simply supported plate ($N = 71 \times 71$, $r = 12.1$).

Fig. 5 shows the perfect match between the vibration displacement response predictions of DSC–MS approach and analytical expression given in Eq. (33) for the frequency $f = 100$ Hz.

4.3.2. *Vibration displacement response of a thin plate*

Analytical expression of the non-dimensional natural frequency parameter of a simply supported thin plate is given as [41]

$$\Omega_{m,n} = \pi^2(m^2 + n^2), \quad m, n = 1, 2, 3, \ldots \tag{36}$$

In the present analysis, the plate was discretized by $N = 71 \times 71$ grid points and discretization parameter r was chosen as 12.1. The plate with the side lengths of 1 m × 1 m has the following parameters: $\rho = 7900\,\mathrm{kg/m^3}$, $h = 0.001$ m, $E = 2.1 \times 10^{11}\,\mathrm{N/m^2}$. Fig. 6 displays the relative error of the first 4761 modes ($P = 4761$) of the simply supported plate predicted by the DSC, corresponding up to almost 21 200 Hz. The region including the first 4750 modes can be thought as acceptable frequency range, since the maximum absolute error is approximately 1% here. However, when comparing the predicted results with the analytical frequencies, it was

noticed that after 3253th mode (= 10 355 Hz), having 0.127% error, some predicted natural modes shift to the position of the subsequent analytical modes. This phenomenon arising due to high-modal density causes the loss of some modal information. This numerical illness may be recovered and the upper limit can be extended to higher frequencies by accommodating better computational configurations. For definitely reliable solutions, only up to the first 3253 modes were considered in all the present plate analyses. However, this much mode can be regarded as rather sufficient for an acceptable high-frequency analysis.

Since there is no analytical solution for the vibration response of finite plates, the comparison study has been performed by using the approximate analytical solution of infinite plates. The plate with $1\,\mathrm{m}\times 1\,\mathrm{m}$ dimensions is sufficiently large to approximately simulate an infinite plate. Displacement field of an infinite, thin, transversely vibrating plate subjected to a harmonic point force $F(t)$ applied at the centre is examined by the wave propagation and the response is given with the far-field assumption ($kr\gg 1$) as [42]

$$w(r)\approx\frac{\mathrm{j}F}{8D_0(1+\mathrm{j}\zeta)k^2}\sqrt{\frac{2}{\pi kr}}\,\mathrm{e}^{\mathrm{j}(\omega t-kr+\pi/4)} \tag{37}$$

Here r is the distance between excitation point (x_f,y_f) and observation point (x,y), i.e., $r=\sqrt{(x-x_f)^2+(y-y_f)^2}$, k is the complex wavenumber and for $\zeta\ll 1$ is given as

$$k=k_0-\mathrm{j}\gamma/2 \tag{38}$$

where k_0 is the wavenumber in the absence of damping, $\gamma=\omega\zeta/c_g$ is the damping coefficient and c_g is the group velocity (i.e., $c_g=2\sqrt{\omega}\sqrt[4]{D_0/\rho h}$). It is seen that in Eq. (37) the response leads to an asymptotic behaviour near the excitation point and it yields an infinite value at the excitation point. However, a finite

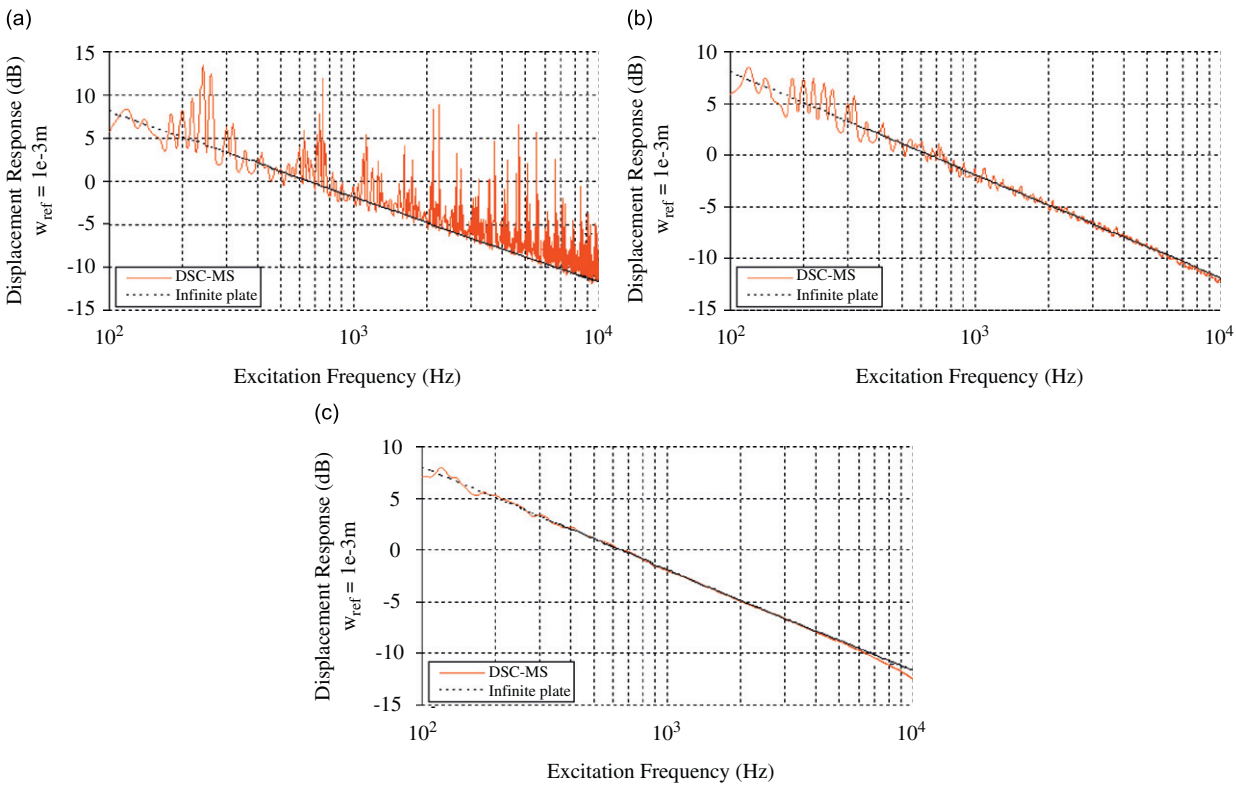

Fig. 7. Comparison of the frequency response spectra predicted by the DSC–MS and approximate analytical solution for infinite plates: (a) $\zeta=0$, (b) $\zeta=0.01$ and (c) $\zeta=0.1$.

maximum value of $w(r)$ can be obtained by determining an initial radius satisfying the condition of $|w(r_0)| = |w(0)|$ as follows:

$$r_0^{-1} \approx \frac{\pi|k|}{2} + \gamma \tag{39}$$

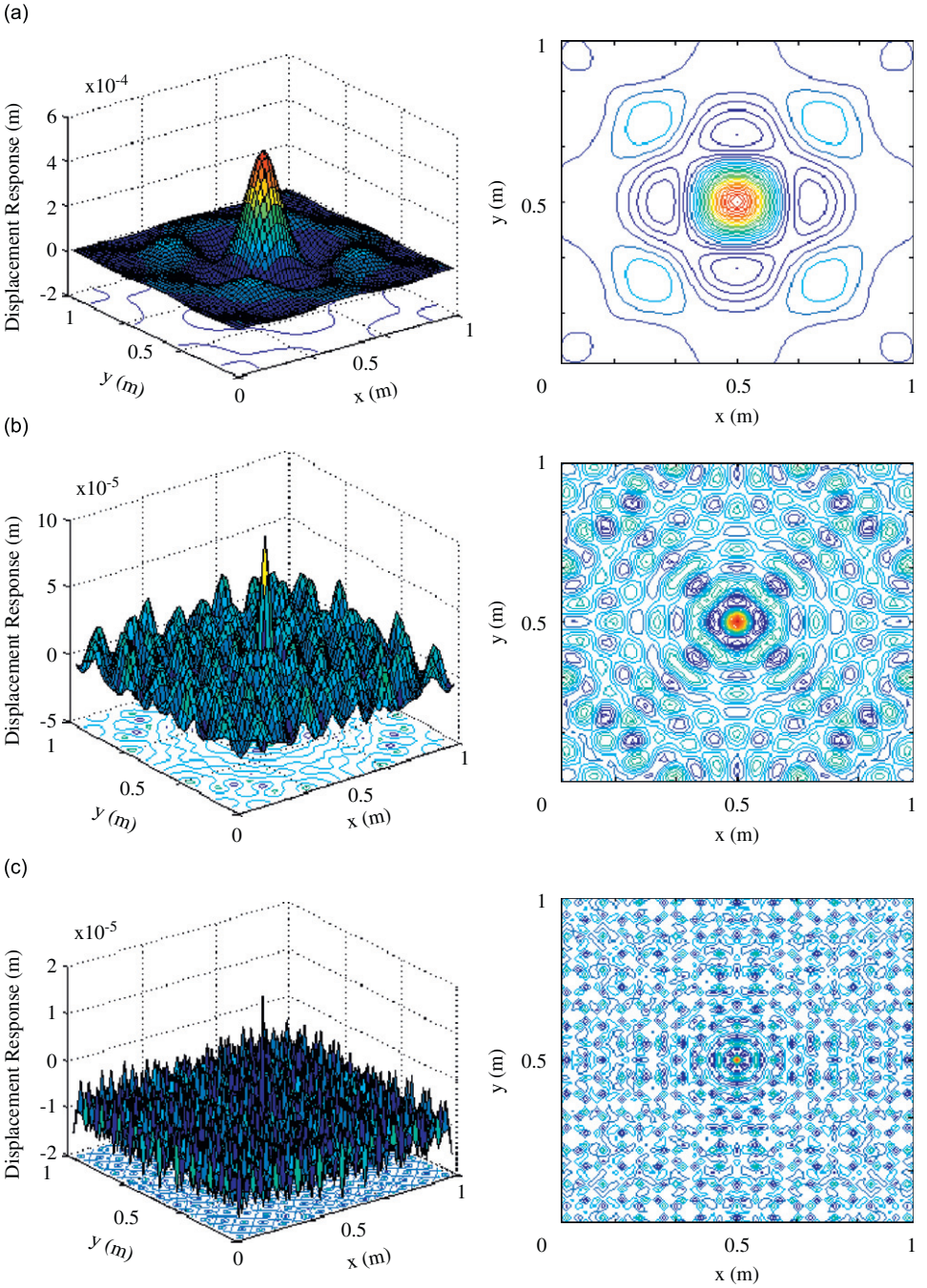

Fig. 8. Spatially distributed vibration response of simply supported thin plate subjected to single central excitation: (a) $f = 100$ Hz, (b) $f = 1000$ Hz and (c) $f = 5000$ Hz (f: excitation frequency).

At that point, the response approximately leads to

$$|w(r_0)| \approx \left| \frac{jF}{8D_0(1+j\zeta)k^2} \right| \tag{40}$$

In this part of the study, the central excitation has an amplitude of $F = 100\,\mathrm{N}$ and its frequency varies between 10^2 and $10^4\,\mathrm{Hz}$. The DSC–MS response at the centre of the plate is presented in Figs. 7(a–c) for three

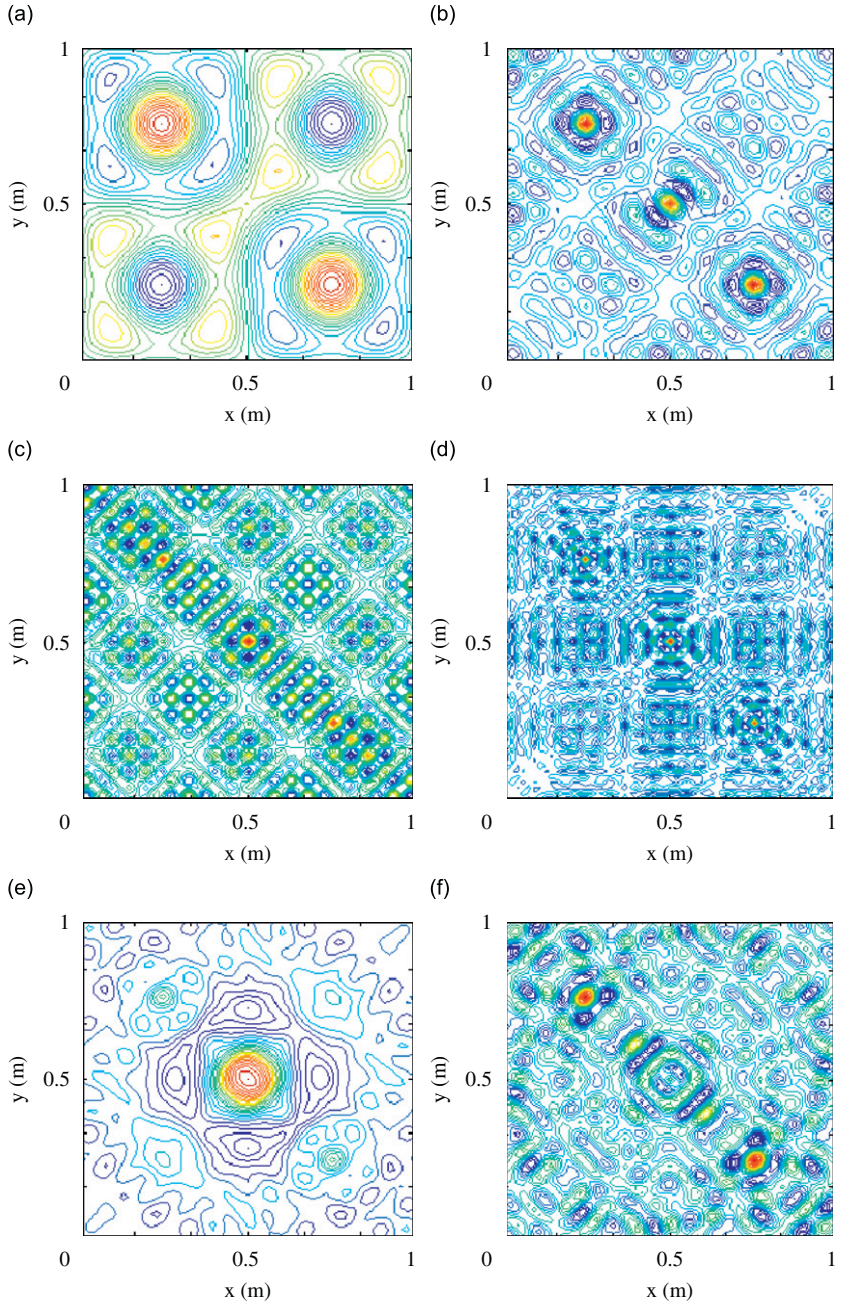

Fig. 9. Spatially distributed vibration response of simply supported thin plate subjected to three different excitations: $e_1 = (0.25, 0.75)\,\mathrm{m}$, $e_2 = (0.5, 0.5)\,\mathrm{m}$, $e_3 = (0.75, 0.25)\,\mathrm{m}$, (a) $f_1 = f_2 = f_3 = 100\,\mathrm{Hz}$, (b) $f_1 = f_2 = f_3 = 1000\,\mathrm{Hz}$, (c) $f_1 = f_2 = f_3 = 2000\,\mathrm{Hz}$, (d) $f_1 = f_2 = f_3 = 5000\,\mathrm{Hz}$, (e) $f_1 = f_3 = 1000\,\mathrm{Hz}$, $f_2 = 100\,\mathrm{Hz}$ and (f) $f_1 = f_3 = 1000\,\mathrm{Hz}$, $f_2 = 2000\,\mathrm{Hz}$ (e_1, e_2, e_3: excitation locations, f_1, f_2, f_3: excitation frequencies).

internal damping factors $\zeta = 0$, 0.01 and 0.1, respectively together with analytical solutions. It is observed in Fig. 7 that DSC–MS results accurately follow the general tendency of the infinite plate response. Since Eq. (40) does not include natural frequency information, the response of infinite plate exhibits a decreasing smooth line with increasing excitation frequency. However, the DSC–MS predicts the response peaks corresponding to natural modes of undamped system discretely as shown in Fig. 7(a). When damping is included, response peaks rapidly disappear (Fig. 7(b)) and DSC–MS results become perfectly matching with the analytical solutions for higher internal damping factors (Fig. 7(c)).

4.4. Numerical applications for discrete response analysis of thin plates

In all numerical applications, the same plate and DSC discretization parameters given in the verification study were used. However, for the spatial and frequency response analyses, fully simply supported and fully clamped boundary conditions were considered, respectively.

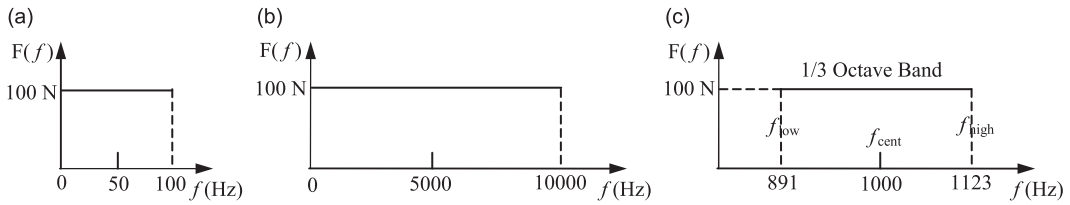

Fig. 10. Time-harmonic excitation force spectra: (a) ideal white noise (0–100 Hz), (b) ideal white noise (0–7500 Hz), (c) 1/3 octave band-limited white noise ($f_{low} = 891$ Hz, $f_{cent} = 1000$ Hz, $f_{high} = 1123$ Hz).

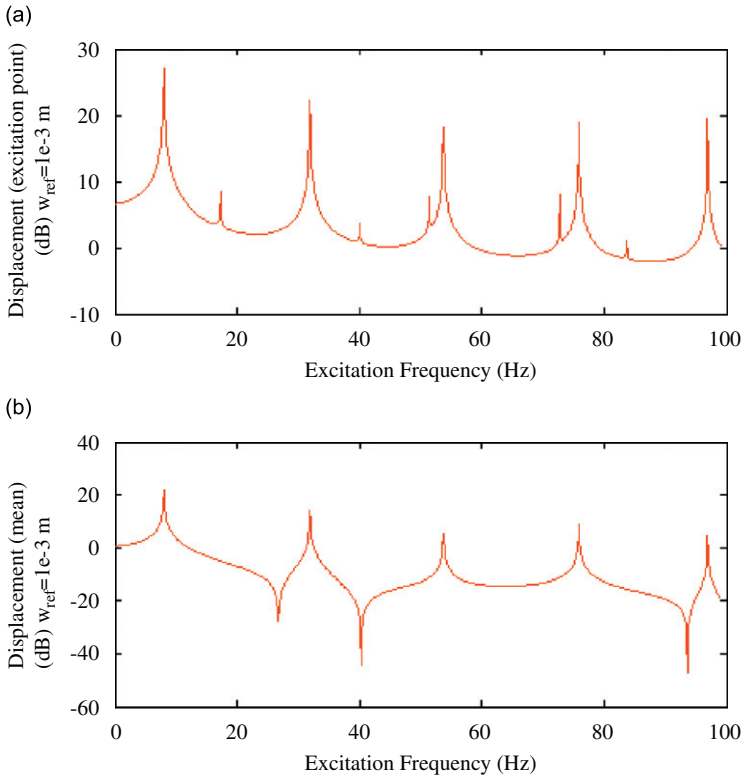

Fig. 11. Frequency response spectra of the plate subjected to central harmonic point force acting at 0–100 Hz: (a) displacement of the excitation point and (b) mean (spatially averaged) displacement.

4.4.1. Spatial response analysis

DSC–MS approach was used for spatially distributed displacement response of fully simply supported undamped thin plate subjected to time-harmonic point forces with different frequency content and having an amplitude of $F = 100$ N. Figs. 8(a–c) show the spatially distributed response of the plate to the single harmonic central excitations at 100, 1000 and 5000 Hz frequencies, respectively. Fig. 9 presents response contours of the plate subjected to three point forces with several frequencies and frequency combinations. These embroidered contours show the versatility of the DSC–MS on predicting spatially distributed response field.

4.4.2. Frequency response analysis

The frequency response analysis of a fully clamped thin plate was performed by DSC–MS approach for the time-harmonic excitation forces for which frequency spectra are given in Fig. 10. The analysis included low, mid and high-frequency regions. The excitation forces were applied to the centre of the plate. Firstly, an excitation in the form of ideal white noise throughout 0–100 Hz as shown in Fig. 10(a) was applied. In this analysis, $P = 25$ modes (= 8.9357–113.79 Hz) were sufficiently contributed to the response. Secondly, an excitation again in the form of ideal white noise but in a much wider range, throughout 0–10 000 Hz, was considered (Fig. 10(b)). Finally, for high-frequency band analysis, a 1/3 octave band of the previous excitation at the 1000 Hz centre frequency was applied (Fig. 10(c)). In the last two cases, $P = 3253$ modes (= 8.9357–10 561 Hz) were taken into account.

Fig. 11 shows the frequency response of the undamped plate to the first excitation. The resonant modes are clearly observed as disturbances for the excitation point response in Fig. 11(a). Since spatial

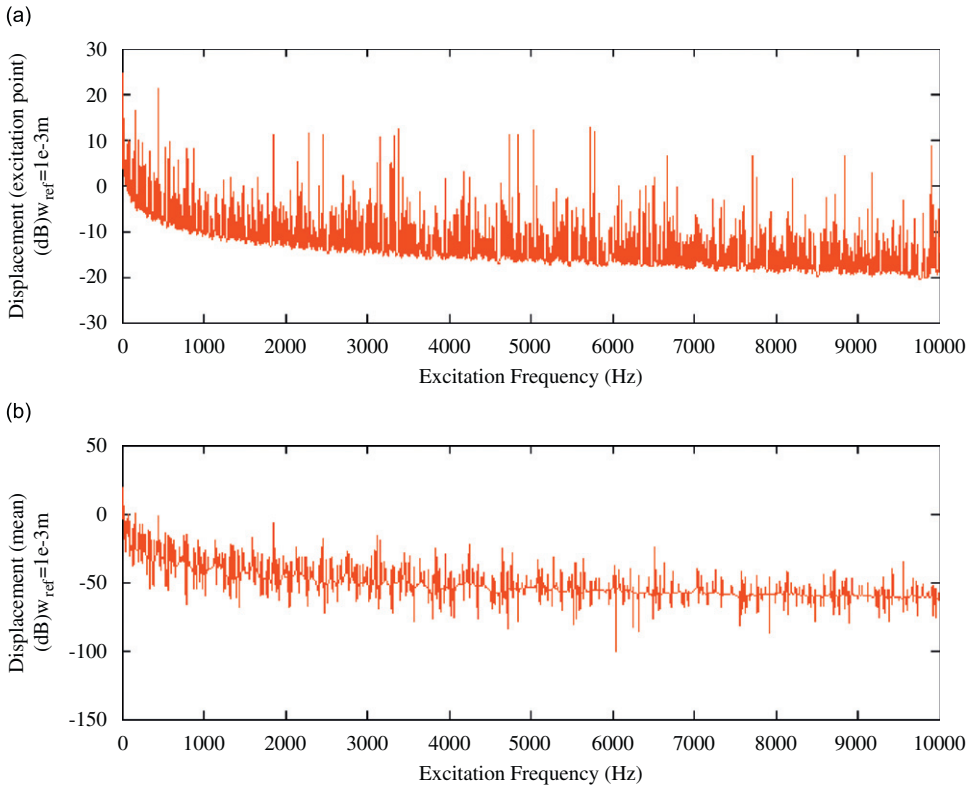

Fig. 12. Frequency response spectra of the plate subjected to a central harmonic point force acting at 0–10000 Hz: (a) displacement of the excitation point and (b) mean (spatially averaged) displacement.

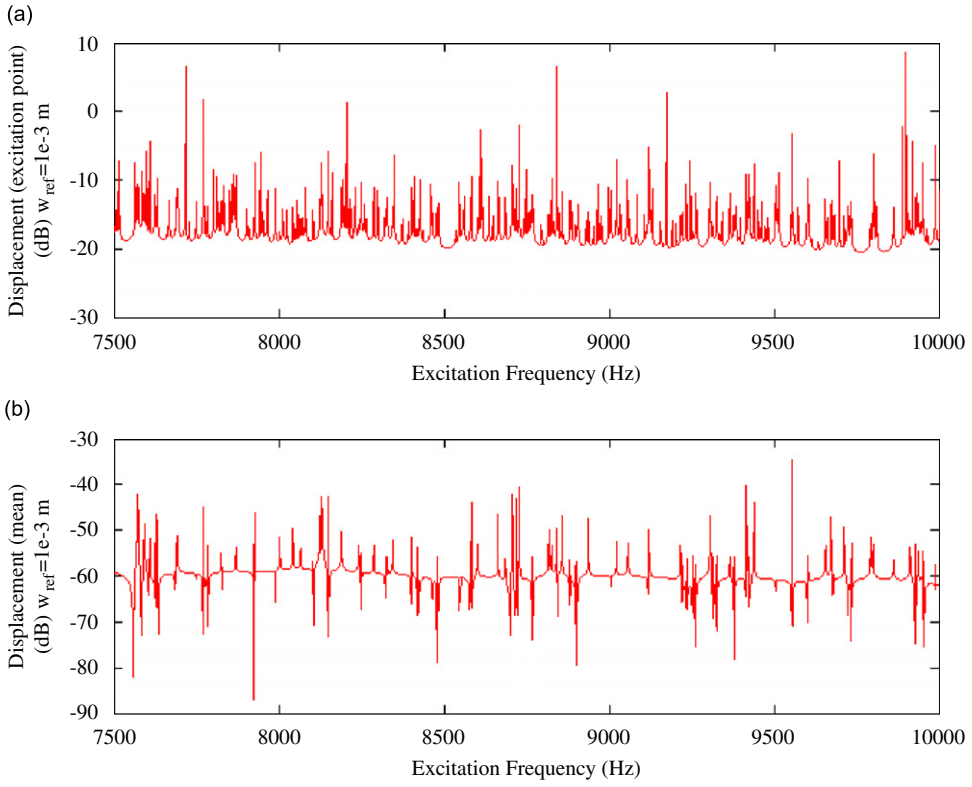

Fig. 13. The focused part of Fig. 12 in the range of 7500–10000 Hz: (a) displacement of the excitation point and (b) mean (spatially averaged) displacement.

averaging causes some weak modal information to be lost, the mean value spectrum in Fig. 11(b) includes only stronger modes.

The response spectra of the undamped plate to the second excitation are given in Fig. 12. It is clearly seen that the DSC–MS is capable of predicting vibration response for the entire frequency range (0–10 000 Hz). In contrast to the smooth response predicted by conventional high-frequency methods, the present scheme yields discrete high-frequency response. The spectra at high frequencies can be better visualized by focusing into 7500–10000 Hz and 9900–10000 Hz frequency ranges as displayed in Figs. 13 and 14, respectively.

The analysis in a limited frequency band shown in Fig. 10(c) for the last application is generally performed by energy-based methods. These methods use the modal energy within a bandwidth to predict an average response along the band. However, in order for these methods to be valid in a frequency region, the considered band must include sufficient number of modes, i.e. the band must have high-modal density. The DSC–MS results obtained for undamped ($\zeta = 0$) and slightly damped ($\zeta = 0.01$) plates are presented in Fig. 15. The modal overlap count for plates can be derived by using Eqs. (31) and (32):

$$\mathrm{MO} = \frac{A_s}{2D}\zeta f_c \tag{41}$$

For $\zeta = 0.01$ and $f_c = 1000$ Hz, MO is calculated as 3.2047; that is greater than Rabbiolo's plate criterion $\overline{\mathrm{MO}} = 2.5$. Therefore, the frequency band with the 1000 Hz centre frequency may be regarded as high-frequency band for the plate at hand. In Fig. 15, it is clearly seen that undamped high-frequency behaviour predicted by the DSC–MS yields the discrete response peaks as much as accurately obtained in the

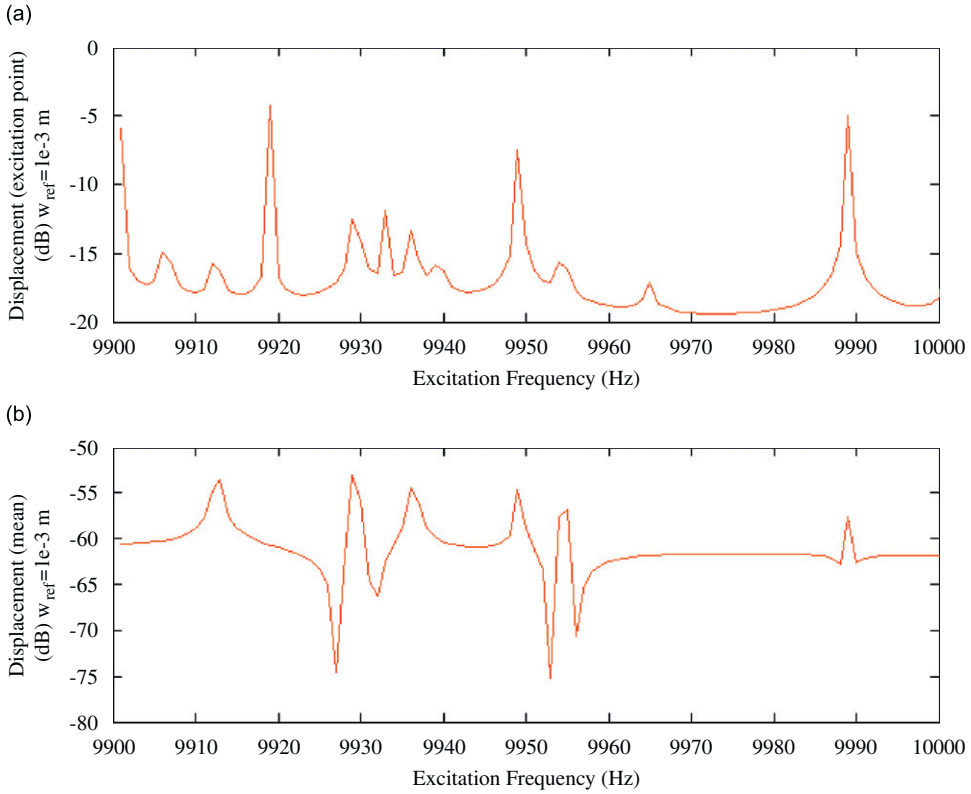

Fig. 14. The focused part of Fig. 12 in the range of 9900–10000 Hz: (a) displacement of the excitation point and (b) mean (spatially averaged) displacement.

low-frequency analysis. However, the damping decreases resonance peaks and therefore the response spectra provide weak modal information. In practice, all systems have damping and for a realistic design, damping behaviour must be adapted to the vibro-acoustic model. The modal content of any real high-frequency system can be discretely obtained by the DSC–MS. The other advantage of the present scheme is that it does not require any pre-condition for the modal density and damping.

5. Conclusion

Available high-frequency approaches are generally based on energy equilibrium between substructures or structural elements. These methods consider average prediction of energy as system variable to describe the response level. Therefore, they disregard modal information and thus, loose discrete response behaviour. This lack of information may cause unrealistic results and leads to unreliable designs.

In the present study, a novel scheme "DSC–MS approach" was introduced for the prediction of spatially distributed and discrete frequency response of structures subjected to time-harmonic point forces. The comparisons with the analytical solutions of thin beams and plates showed that the present approach can be reliably used for high-frequency vibration analysis. By this powerful approach, it became possible to disregard the energetic parameters and to consider primary response variables for high frequencies. The DSC–MS predicts the response spectra with a perfect resolution. The method can be reliably used for the entire frequency ranges without any pre-conditioning of modal density and damping. DSC–MS approach promises new horizons on recovering uncertainties at high frequencies by providing basic system characteristics.

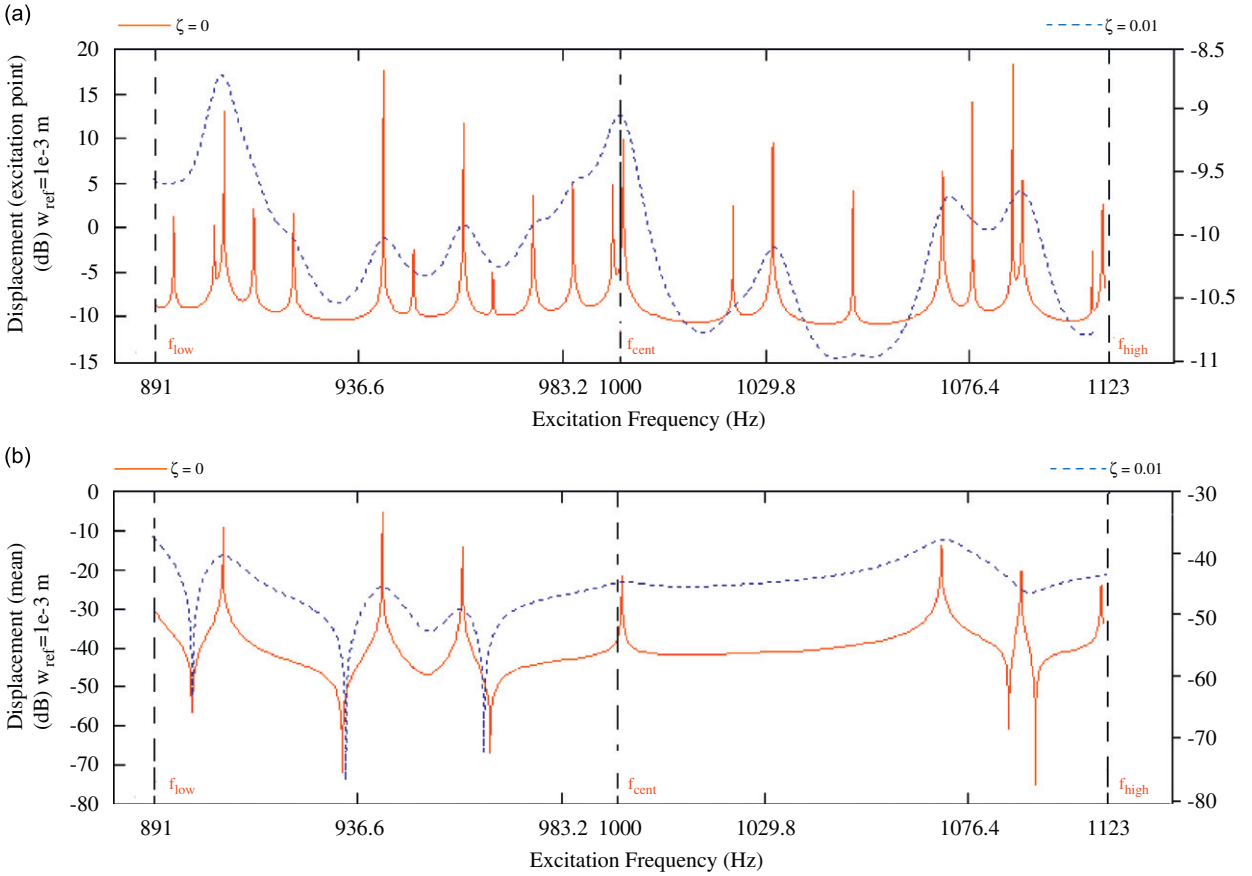

Fig. 15. Frequency response spectra of the plate subjected to central harmonic point force acting at 1000 Hz with 1/3 octave band: (a) displacement of the excitation point and (b) mean (spatially averaged) displacement.

Appendix A. Supporting Information

Supplementary data associated with this article can be found in the online version at doi:10.1016/j.jsv.2008.08.031.

References

[1] G. Rabbiolo, R.J. Bernhard, F.A. Milner, Definition of a high-frequency threshold for plates and acoustical spaces, *Journal of Sound and Vibration* 277 (2004) 647–667.
[2] R.H. Lyon, R.G. DeJong, *Theory and Application of Statistical Energy Analysis*, Butterworth-Heinemann, USA, 1995.
[3] F. Bitsie, The Structural-Acoustic Energy Finite Element Method and Energy Boundary Element Method, PhD Thesis, Purdue University Graduate School, 1996.
[4] F. Han, R.J. Bernhard, L.G. Mongeau, Energy flow analysis of vibrating beams and plates for discrete random excitations, *Journal of Sound and Vibration* 208 (5) (1997) 841–859.
[5] F. Han, R.J. Bernhard, L.G. Mongeau, Prediction of flow-induced structural vibration and sound radiation using energy flow analysis, *Journal of Sound and Vibration* 227 (4) (1999) 685–709.
[6] S. Wang, High Frequency Energy Flow Analysis Methods: Numerical Implementation, Applications and Verification, PhD Thesis, Purdue University Graduate School, 2000.
[7] R.S. Langley, A wave intensity technique for the analysis of high frequency vibrations, *Journal of Sound and Vibration* 159 (3) (1992) 483–502.
[8] M.J. Smith, A hybrid energy method for predicting high frequency vibrational response of point-loaded plates, *Journal of Sound and Vibration* 202 (3) (1997) 375–394.

[9] A. Carcaterra, A. Sestieri, Complex envelope displacement analysis: a quasi-static approach to vibrations, *Journal of Sound and Vibration* 201 (2) (1997) 205–233.
[10] A. LeBot, A vibro-acoustic model for high frequency analysis, *Journal of Sound and Vibration* 211 (4) (1998) 537–554.
[11] K.S. Chae, J.G. Ih, Prediction of vibrational energy distribution in the thin plate at high-frequency bands by using the ray tracing method, *Journal of Sound and Vibration* 240 (2) (2001) 263–292.
[12] G.W. Wei, Discrete singular convolution for the solution of Fokker-Plank equation, *Journal of Chemical Physics* 110 (18) (1999) 8930–8942.
[13] G.W. Wei, Discrete singular convolution for the sine-Gordon equation, *Physica D* 137 (2000) 247–259.
[14] G.W. Wei, Wavelets generated by using discrete singular convolution, *Journal of Physics A* 33 (2000) 8577–8596.
[15] G.W. Wei, Solving quantum eigenvalue problems by discrete singular convolution, *Journal of Physics B* 33 (2000) 343–352.
[16] G.W. Wei, Discrete singular convolution for beam analysis, *Engineering Structures* 23 (2001) 1045–1053.
[17] G.W. Wei, Vibration analysis by using discrete singular convolution, *Journal of Sound and Vibration* 244 (3) (2001) 535–553.
[18] G.W. Wei, A new algorithm for solving some mechanical problems, *Computational Methods in Applied Mechanics and Engineering* 190 (2001) 2017–2030.
[19] G.W. Wei, Y.B. Zhao, Y. Xiang, The determination of natural frequencies of rectangular plates with mixed boundary conditions by discrete singular convolution, *International Journal of Mechanical Sciences* 43 (2001) 1731–1746.
[20] G.W. Wei, Y.B. Zhao, Y. Xiang, Discrete singular convolution and its application to the analysis of plates with internal supports. Part 1: theory and algorithm, *International Journal for Numerical Methods in Engineering* 55 (2002) 913–946.
[21] Y. Xiang, Y.B. Zhao, G.W. Wei, Discrete singular convolution and its application to the analysis of plates with internal supports. Part 2: applications, *International Journal for Numerical Methods in Engineering* 55 (2002) 947–971.
[22] Y.B. Zhao, G.W. Wei, Y. Xiang, Plate vibrations under irregular internal supports, *International Journal of Solids and Structures* 39 (2002) 1361–1383.
[23] Y.B. Zhao, G.W. Wei, DSC analysis of rectangular plates with non-uniform boundary conditions, *Journal of Sound and Vibration* 255 (2) (2002) 203–228.
[24] S. Zhao, G.W. Wei, Y. Xiang, DSC analysis of free-edged beams by an iteratively matched boundary method, *Journal of Sound and Vibration* 284 (2005) 487–493.
[25] Y. Hou, G.W. Wei, Y. Xiang, DSC–Ritz method for the free vibration analysis of Mindlin plates, *International Journal for Numerical Methods in Engineering* 62 (2005) 262–288.
[26] Ö. Civalek, Numerical analysis of free vibrations of laminated composite conical and cylindrical shells: Discrete singular convolution (DSC) approach, *Journal of Computational and Applied Mathematics* 205 (2007) 251–271.
[27] Ö. Civalek, Free vibration and buckling analyses of composite plates with straight-sided quadrilateral domain based on DSC approach, *Finite Elements in Analysis and Design* 43 (13) (2007) 1013–1022.
[28] Ö. Civalek, A parametric study of the free vibration analysis of rotating laminated cylindrical shells using the method of discrete singular convolution, *Thin Walled Structures* 45 (7-8) (2007) 692–698.
[29] A. Seçgin, C. Atas, A.S. Sarıgül, Investigation of the effects of material and fiber orientation angles on the modal characteristics of thin FML composite plates by using discrete singular convolution (DSC) approach, Fourth Ankara International Aerospace Conference, Article No: AIAC-2007-045, Ankara, Turkey, 2007.
[30] A. Seçgin, A.S. Sarıgül, Free vibration analysis of symmetrically laminated thin composite plates by using discrete singular convolution (DSC) approach: algorithm and verification, *Journal of Sound and Vibration* 315 (1–2) (2008) 197–211.
[31] G.W. Wei, Y.B. Zhao, Y. Xiang, A novel approach for the analysis of high-frequency vibrations, *Journal of Sound and Vibration* 257 (2) (2002) 207–246.
[32] Y.B. Zhao, G.W. Wei, Y. Xiang, Discrete singular convolution for the prediction of high frequency vibration of plates, *International Journal of Solids and Structures* 39 (2002) 65–88.
[33] C.W. Lim, Z.R. Li, G.W. Wei, DSC–Ritz method for high-mode frequency analysis of thick shallow shells, *International Journal for Numerical Methods in Engineering* 62 (2005) 205–232.
[34] C.H.W. Ng, Y.B. Zhao, G.W. Wei, Comparison of discrete singular convolution and generalized differential quadrature for the vibration analysis of rectangular plates, *Computer Methods in Applied Mechanics and Engineering* 193 (2004) 2483–2506.
[35] S. Timoshenko, D. Young, W. Weaver, *Vibration Problems in Engineering*, Wiley, New York, 1971.
[36] C.R. Fredö, A SEA-like approach for the derivation of energy flow coefficients with a finite element model, *Journal of Sound and Vibration* 199 (4) (1997) 645–666.
[37] R.N. Coppolino, Finite element models, in: C.M. Harris, A. Piersoll (Eds.), *Shock and Vibration Handbook*, McGraw-Hill, Newyork, 2002 Part II (Chapter 28).
[38] F.J. Fahy, A.D. Mohammed, A study of uncertainty in applications of SEA to coupled beam and plate systems, part I: computational experiments, *Journal of Sound and Vibration* 158 (1) (1992) 45–67.
[39] L.W. Qian, G.W. Wei, A note on regularized Shannon's sampling formulae, Preprint, arXiv:math. 2000, SC/0005003.
[40] W.F. Stokey, Vibration of systems having distributed mass and elasticity, in: C.M. Harris, A. Piersoll (Eds.), *Shock and Vibration Handbook*, McGraw-Hill, New York, 2002 (Chapter 7).
[41] A.W. Leissa, *Vibration of Plates*, NASA, Washington, DC, 1969.
[42] L. Cremer, M. Heckl, E.E. Ungar, *Structure-borne Sound*, Springer, Berlin, 1988.